







The Sensitivity of Urban Pluvial Flooding to the Temporal Distribution of Rainfall Within Design Storms

¹School of Civil Engineering, University of Leeds, Leeds, UK | ²Institute of Climate and Atmospheric Science, University of Leeds, Leeds, UK

Correspondence: Molly Asher (gy17m2a@leeds.ac.uk)

Received: 29 January 2024 | Revised: 18 March 2025 | Accepted: 20 June 2025

Funding: This work was supported by Natural Environment Research Council, NE/S007458/1.

Keywords: design profiles | extreme events | flood estimation | hyetographs | modelling | pluvial flooding | rainfall | temporal distribution

ABSTRACT

The risk posed globally by pluvial flooding to people and properties is growing due to urbanisation, infrastructure development and intensification of rainfall due to climate change. Whilst tools to model pluvial flood hazard have also advanced, there remains a knowledge gap around whether design storms used in modelling adequately represent the temporal distribution of rainfall within the extreme convective storms which drive flooding. In the UK, the industry standard design storm considers rainfall events to always have a singular, central intensity peak. Study of UK extreme rainfall observations suggests that loading of rainfall towards the start or end of events is in fact more common. This study highlights the sensitivity of pluvial flood extent, hazard and timing to the shape of the design rainfall profile for two urban catchments in northern England. We demonstrate that for events with the same accumulated rainfall depth, there is up to a 25% increase in total flood-affected area with a back-loaded compared to a front-loaded profile. Failing to account for the variability in event profile shapes observed in real events may result in substantial inaccuracies in the design of flood risk management solutions, leading to both underestimation and overestimation of the required measures.

1 | Introduction

Flooding is the most frequently occurring and harmful natural hazard globally (Jenkins et al. 2018; Razavi et al. 2020). In England, pluvial flooding is the most widespread form of flooding, placing roughly 3.2 million properties at risk (Environment Agency 2021). Pluvial flooding—or surface water flooding as it is commonly known in the UK—occurs when the volume of rainfall exceeds the absorption capacity of the ground and the storm water drainage capacity (Archer and Fowler 2018). It generally occurs in urban settings, which have a higher proportion of impermeable surfaces that preclude the natural processes that moderate floods in rural environments. The fast runoff and rapid response times in urban hydrology mean that pluvial flooding is more directly dependent than fluvial flooding on the

characteristics of rainfall at smaller spatial and temporal scales (Ochoa-Rodriguez et al. 2015; Peleg et al. 2017).

The influence of the temporal structure of rainfall has been a persistent question in hydrology for many years (Dawdy and Bergmann 1969; Singh 1997; Woods and Sivapalan 1999). There has been substantial exploration into the temporal and spatial resolution of rainfall data required to faithfully represent the dynamics of storm events that influence urban hydrological processes. Temporal resolutions of between one and 5 min have been posited by several authors as a prerequisite for modelling certain processes (Schilling 1991; Einfalt et al. 2004; Berne and Krajewski 2013). Much work has focused on providing data at this resolution through radar products (Einfalt et al. 2004; Thorndahl et al. 2017; Bruni et al. 2015), and stochastic rainfall

[Correction added on 18 September 2025, after first online publication: The name of the author Steven Boïng was corrected to Steven Böing in this version.]

This is an open access article under the terms of the Creative Commons Attribution License, which permits use, distribution and reproduction in any medium, provided the original work is properly cited.

© 2025 The Author(s). Journal of Flood Risk Management published by Chartered Institution of Water and Environmental Management and John Wiley & Sons Ltd.

generators, which produce sets of synthetic rainfall events that closely mimic the fine scale spatial and temporal structure of real rainfall events (Peleg et al. 2017; Zhu et al. 2018; Paschalis et al. 2014; Gabellani et al. 2007).

Although considerable improvements have been made in these areas, it remains standard practice to use design storms in flood modelling. These are idealised rainfall events with greatly simplified characteristics (Butler and Davies 2004). They are advantageous as they avoid the need to model multiple individual historical rainfall events in a particular catchment, thereby reducing the computational burden. They also allow a standardised approach to assessing the impact of extreme rainfall, including events with magnitudes higher than have ever been experienced in reality (Marsalek and Watt 1984; Balbastre-Soldevila et al. 2019). The total event accumulated rainfall depth is calculated through statistical analyses of historical rainfall data and is generated for different durations and return periods. This rainfall depth is then distributed over time using a hyetograph which represents the time varying distribution of rainfall during a storm. The way in which the shape of the hyetograph is specified and the impact of this on the resulting flood hazard is the focus of this work.

There are a number of different approaches to specifying hyetographs. These are outlined in detail by Te Chow et al. (1988), Veneziano and Villani (1999), and Balbastre-Soldevila et al. (2019), amongst others. The approaches can be loosely categorised as: summary (generalising temporal distributions from observed events); geometric (constructing simple geometric shapes, for example, a triangle or rectangle, with intensities drawn from an IDF (intensity duration frequency) curve derived from historical records); or stochastic (generalising temporal distributions from events from stochastic rainfall generators).

In the UK, the industry standard approach to flood hazard modelling is to use one of two design hyetographs specified in the Flood Estimation Handbook (FEH) (Faulkner 1999). The FEH hyetographs are both symmetrical with a central peak in intensity and bear a close similarity to the Chicago Design storm, which is widely applied in other countries (Keifer and Chu 1957; Watt and Marsalek 2013; Yang et al. 2020). The FEH profiles are applied regardless of the event duration or return period, with a summer profile, which is more sharply peaked and with a higher magnitude, advised for use in urban areas and a winter profile, which has a more shallow peak, recommended for rural catchments (Faulkner 1999). The FEH profiles are best described as summary hyetographs and were derived by study and generalisation of just 80 summer (May to October) and 32 winter (November to April) storms of 24-h duration occurring between 1961 and 1970. The generalisation process is described in detail by Villalobos Herrera, Blenkinsop, Guerreiro, Dale, et al. (2023). Importantly, in addition to the stages typical of generating summary hyetographs, the peak of each event is also shifted to the centre. This ensures that when summary profiles are derived from averaging across multiple observed rainstorms, there is always a temporally central peak in intensity. Whilst much of the flood estimation methods associated with the FEH have been updated more recently, the hyetographs have essentially not been revised in the last 50 years (minor modifications in ReFH2.3 are discussed in Appendix A).

Recent research indicates that the FEH hyetographs are not representative of the true variety in the timing of peak intensity in observed storms. A set of ~70,000 UK independent rainstorms ranging from sub-hourly to daily durations were identified by Villalobos Herrera, Blenkinsop, Guerreiro, and Fowler (2023) using a new storm identification algorithm. These storms were used to trial an alternative approach to deriving summary hyetographs which removes the centring step applied in the FEH methodology. Rather, the positioning of the peak is made fundamental to the hyetograph classification, with profiles classed as front-loaded, centred or back-loaded. Importantly, Villalobos Herrera, Blenkinsop, Guerreiro, Dale, et al. (2023) find that just 23% of the observed storms have a central peak in intensity. This provides evidence that the majority of UK extreme storms are fundamentally different to design storms produced with the FEH hyetographs, and calls into question the validity of their continued application in UK flood modelling approaches.

There is an inherent implication in the recognition of the sensitivity of urban hydrological models to the temporal resolution of rainfall used in continuous simulations, that the temporal distribution of rainfall in design storms must also influence the catchment response. A number of studies have also explicitly tested this. An early study by Lambourne and Stephenson (1987) compares the peaks and volumes of runoff produced by four simple geometric design storm shapes in an urban catchment in South Africa, finding that triangular and bimodal design storm profiles well approximate the runoff from real rainfall events. Nguyen et al. (2002) assess the runoff peaks and volumes produced by seven commonly used design storms in Canada, but struggle to identify the 'best' design storm, as different design storm options perform best for different runoff parameters. Balbastre-Soldevila et al. (2019) investigate the hydrographs produced by 11 widely applied design storms for a rainfall-runoff model of an urban catchment in Valencia, and show that the choice of profile substantially impacts the predicted peak flow and flood volume. Krvavica and Rubinic' (2020) compare the performance of six design storms against two real rainfall events, finding that design storms can have a tendency to smooth out the peaks found in real events, and therefore to underestimate flood risk. Hettiarachchi et al. (2018) apply six temporal patterns frequently used in the USA, for a model of an urban catchment in Minnesota. They highlight that a shift towards more peaky and non-uniform rainfall patterns under climate change will increase the flood risk in urban watersheds. Li et al. (2021) produce a variety of hyetographs for Seoul using Huff curves. They find that storms with later peaks in intensity cause more severe urban inundation impacts. Overall, the conclusions of these research works tend to agree that the storm temporal profile does influence the flooding outcome, but the more specific conclusions vary and depend on the questions tackled.

There are two notable gaps in the existing research on the impact of the temporal distribution of rainfall in design storms on flood risk. First, while studies applying idealised profiles have tested a variety of simple, summary temporal patterns, they have often failed to conduct systematic adjustments to these profiles to assess the consequences of shifting the timing of the peak intensity. Second, there is an absence of research examining realistic observed rainfall profiles within

the context of the UK. This paper builds on the work of Villalobos Herrera, Blenkinsop, Guerreiro, and Fowler (2023) to provide evidence on the sensitivity of urban hydrological response in a UK catchment to the distribution of rainfall in design profiles. Specifically, the aims of this paper are to use rain-on-grid flood modelling to test the sensitivity of flood extent, depth and timing in an urban catchment to:

- 1. The timing of the peak intensity in an idealised, single-peaked design storm.
- 2. The range of temporal distributions in physically realistic hyetographs, and to quantify how these outcomes differ from using a single-peaked design storm.

2 | Methods

2.1 | The Study Catchments

Wyke Beck and Lin Dyke are two suburban catchments in east Leeds (Figure 1a), in northern England (Figure 1b). Both catchments have historically been affected by pluvial flooding, making them typical examples of urbanised or partially urbanised pluvial flood risk catchments in the UK. Wyke Beck covers 33.6 km² and has a large (63%) urban share, including numerous populous Leeds suburbs. It also includes a smaller proportion (36%) of green spaces, such as woodland and parks, and a small (1%) contribution from the permanent water in Waterloo Lake, to the north of the catchment, and Wyke Beck, a tributary of the River Aire (Figure 1c). Lin Dyke covers 22.9 km²; the majority (69%) of the catchment is rural land

uses, such as farmland and woodland, with a smaller proportion (27%) made up of urban and suburban land uses around the settlements of Kippax and Garforth. The remainder of the catchment (4%) is permanent water, which is primarily found in the wetlands in the downstream area of the catchment, which drain into the River Aire (Figure 1c). Both catchments have the highest elevations in the northern catchment headwaters. In Wyke Beck, the highest elevations are greater than those in Lin Dyke (Figure 1d).

2.2 | The Flood Inundation Model

A 2D hydraulic rain-on-grid model is run in Hec-Ras model software (v6.4.1) using the 2D unsteady diffusion wave equation set (Brunner 2016). Hec-Ras has been used in a multitude of pluvial flood modelling studies (e.g., Costabile et al. 2021; Yalcin 2020; Singh et al. 2023; Rangari et al. 2019). A diffusive solver was chosen over the more accurate full Shallow Water Equation (SWE) solver for computational efficiency, given the need for multiple model runs. This was deemed appropriate as our study focuses on relative flood hazard comparison at the catchment scale, rather than building-scale accuracy, where SWEs provide greater precision (Costabile et al. 2017). Rainon-grid modelling applies a rainfall input to each grid cell and simulates the movement of this water overland. Topography is defined with a Digital Elevation Model (DEM) and determines flow pathways and water ponding locations. Rain-ongrid modelling is a widely accepted approach to modelling pluvial flooding and was applied in the production of the Risk of Flooding From Surface Water (RoFSW) map (Environment

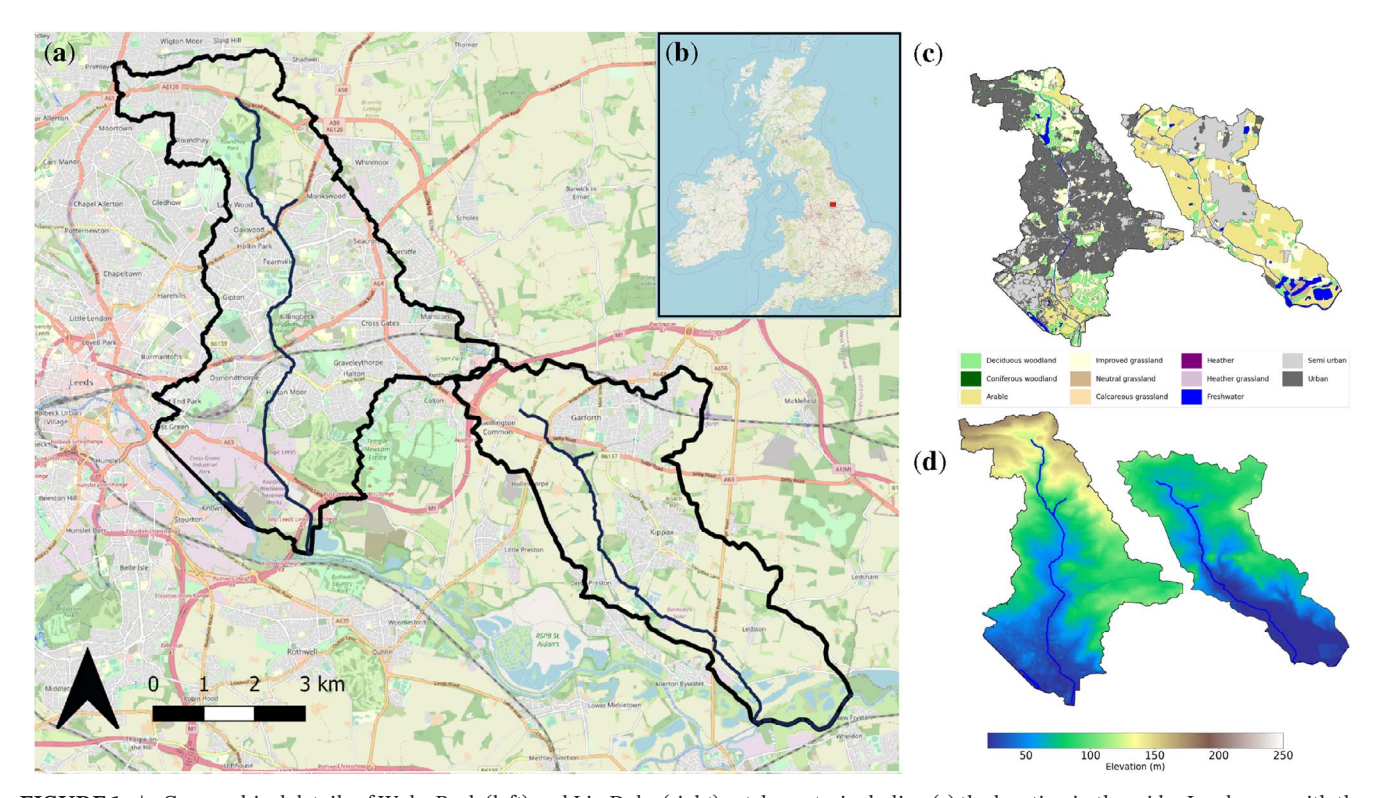


FIGURE 1 | Geographical details of Wyke Beck (left) and Lin Dyke (right) catchments, including (a) the location in the wider Leeds area with the main watercourse marked, (b) the location in the UK, (c) land use, and (d) topography.

Agency 2019). Despite this, there are some limitations to rainon-grid modelling. In particular, it is common practice to not explicitly represent urban drainage and infiltration, and instead to reduce rainfall rates before applying them to the model in order to approximate these losses. A large number of factors influence drainage system outcomes in urban environments, and consequently drainage system response to rainfall events is inherently non-linear. The simplified loss removal process applied here is incapable of capturing this non-linearity, and this is an important source of uncertainty in our model results. The impact of this on our ability to assess the impact of the temporal profile on flood hazard is discussed in Section 4.

Existing flood models are used for both Lin Dyke (Beadle 2021) and Wyke Beck (Singh et al. 2023) catchments. Both models use a computational mesh with a general resolution of 10 m. Testing showed that further mesh refinement had negligible impact on flood extent, so this resolution was chosen as a balance between accuracy and computational efficiency. To improve accuracy along the main watercourse, the mesh was refined using a break line, allowing for more precise representation of channel flows without globally reducing the mesh size. Furthermore, Hec-Ras uses subgrid topographical representation, meaning that the high-resolution detail of the base DEM is preserved within each mesh cell. As a result, even with a 10 m mesh, fine-scale terrain features are effectively incorporated into the hydraulic calculations. The land use data for Lin Dyke is the UK CEH 2019 Land Cover Map (Morton et al. 2020) and the OS MasterMap for Wyke Beck. The roughness coefficients are specified based on the land cover type for each cell, using values suggested for use in Hec-Ras guidance (US Army Corps of Engineers 2020). Both models use a 'bare earth' LiDAR DEM, at a resolution of 1 m for Lin Dyke and 2 m for Wyke Beck (Environment Agency 2021). Buildings alter surface runoff routes, and the DEM is adjusted by raising the terrain within building footprints to roof height using OS MasterMap data. Further adjustments are made to the DEM to ensure that hydraulic structures, such as bridges and culverts, are not unrealistically blocking the flow completely (Beadle 2021; Singh et al. 2023; Houston et al. 2011; Wang et al. 2023). The OS Open Rivers data is used to locate areas where the DEM is blocking a watercourse. The watercourse channel is then manually opened by editing the DEM directly with the terrain modification tools in Hec-Ras Mapper to ensure flow is able to pass through unobstructed. The model uses a 'normal depth' boundary with an assumed slope of 0.0003 to allow water to exit the catchment, simplifying flow calculations based on the channel gradient. Although potential backwater effects from high levels in the River Aire are not considered, this is appropriate for short-duration runoff events in this study. The River Aire is much larger and takes days to peak, while runoff in the catchment occurs within hours, meaning backwater effects are unlikely to influence these rapid events.

The models are run for an event time of 70h. The Lin Dyke catchment includes large storage elements at the downstream end, near its River Aire outlet, known as Fairburn Ings. These wetlands were formed by coal mining subsidence and are now a designated RSPB protected local nature reserve (Pickles 2010).

These are slow to fill from upstream inputs, and also slow to later release water. A 70h time was selected to balance model operational time and cost, while ensuring that the hydrological processes happening in the catchment after the storm are adequately captured. To maintain numerical stability, the Courant number must typically be kept at or below 1 (Courant et al. 1967; Rangari et al. 2019). Here, the model uses a variable time step, automatically adjusting it to maintain a Courant value within the range of 0.75 to 2. This allows Hec-Ras to choose an appropriate adaptive time step for the model solution at any given point of the simulation.

2.3 | The Rainfall Data

Pluvial flooding is generally associated with short duration, convective rainfall events (Rudd et al. 2020). A 6-h duration was selected because previous studies (Beadle 2021) identified it as the critical duration for Lin Dyke, meaning it produces the highest peak flows (Davies and Hancock 2015). While the time of concentration, the time for runoff from the furthest point in the catchment to reach the outlet, is sometimes used to identify a relevant event duration for modelling, it does not necessarily correspond to the duration that generates the most severe flooding. Using the critical duration ensures the model captures the worst-case scenario for peak flows, which is the primary focus of this study. Although 6-h perhaps seems long for a summertime convective event, this duration allows for a period of lighter rainfall either side of a convective peak. We modelled a 1-in-100 year return period event. As the middle of three options modelled in the RoFSW map (Environment Agency 2019), we considered this a representative example of a moderately extreme scenario. A 6-h, 1-in-100 year event corresponds to a total accumulated rainfall depth of 59.29 mm in Lin Dyke catchment and 59.25 mm in Wyke Beck. These values are extracted from the FEH web service, which provides accumulated rainfall depths associated with specific durations and return periods for UK catchments.

Design storm profiles are required to translate this accumulated rainfall depth into the hyetographs that form the rainfall input to the flood model. We construct hyetographs, all with the same total event rainfall volume, using the three design storm profile options described below:

- The FEH standard summer profile (Figure 2). This establishes a baseline—or standard—assessment of catchment flood hazard.
- 2. Idealised profiles created by shifting the timing of the FEH profile's peak while retaining its general shape. Each profile has the same peak intensity, allowing changes to flood hazard resulting from the timing of the peak to be studied in isolation from the impact of the size of the peak (Figure 3a).
- 3. Observed profiles summarising observed extremes. Both the timing and magnitude of the peak intensity vary between profiles. This allows quantification of the differences in flood hazard arising from the range of temporal profiles expected to be found amongst UK extreme rainfall events of this duration (Figure 3c).

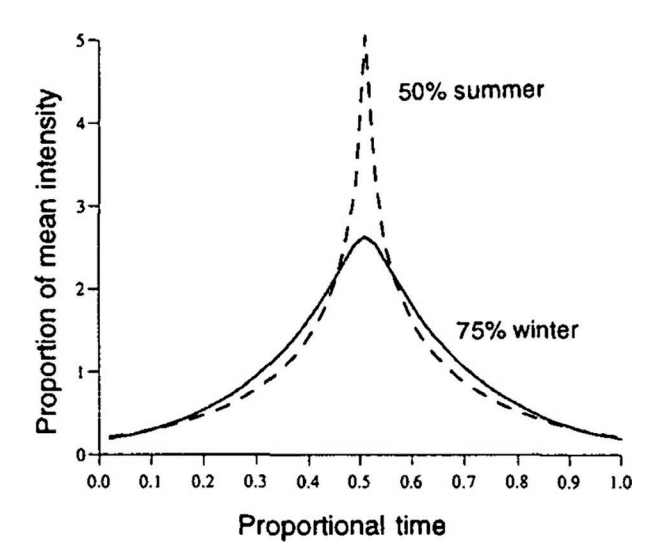


FIGURE 2 | FEH summer design profile, from Faulkner (1999).

At the end of each simulation, the water volume in the model is the same for all profiles (idealised, observed, and FEH): 5.89 million m³ in Lin Dyke and 11.02 million m³ in Wyke Beck.

2.3.1 | FEH Profile

The Revitalised Flood Hydrograph model (ReFH2) software is used to generate the FEH summer design profile for our catchments (black solid line, Figure 3a,b,c).

2.3.2 | Idealised Profiles

We produce an approximated version of the FEH summer design profile (I5) based on the FEH guidance (Kjeldsen 2007). Further details are provided in Appendix A. Eight further idealised profiles are created by shifting the peak of this approximated FEH summer profile in time, but otherwise retaining the shape. Table 1 describes the profiles and the abbreviations used to describe them throughout this research. Four versions (I1-4) are front-loaded (with the peak in intensity occurring during the first half of the event) and four (I6-9) are back-loaded (with the peak in intensity occurring during the second half of the event). The profiles are created through rescaling the time axis before and after the peak. For example, for a front-loaded event, the rainfall curve before the peak is compressed, and after the peak it is stretched. More details on profile construction are given in Appendix B.

2.3.3 | Observed Profiles

We use 15 temporal profiles identified through study of observed rainfall extremes by Villalobos Herrera, Blenkinsop, Guerreiro, Dale, et al. (2023), the abbreviations used to describe them in this research are outlined in Table 1. In earlier research, Villalobos Herrera, Blenkinsop, Guerreiro, and Fowler (2023) extract ~70,000 extreme rainstorms from sub-hourly resolution data from 1279 rain gauges. These storms are responsible for generating annual maximum

rainfall intensities for fixed durations between 0.5 and 24h. In Villalobos Herrera, Blenkinsop, Guerreiro, Dale, et al. (2023), further work is done to capture the most common temporal distribution profiles found amongst the most extreme 10% of these events, subdivided into duration categories defined by them. First, the events are converted to Huff curves. Huff curves represent the accumulated rainfall depth over the course of an event, normalised by the event's total depth and duration (Yin et al. 2016). To enable comparison of events of different durations, all Huff curves are aggregated into 12 segments of equal length, with linear interpolation used to fill in values in cases where some segments are empty. For each of the duration bins, a k-means cluster analysis is then performed on the Huff curves, and a summary profile is defined for each cluster by taking the mean of all the Huff curves assigned to that cluster.

Here, we use 15 summary profiles identified in this way for events between ~2 and 6 h. We construct profiles for a 6h duration, which is thus comprised of 12 time steps of 30 min each. The total rainfall accumulated depth falling in each 30 min time step is assumed to fall at a constant rate, with each minute assigned a rainfall accumulated depth of 1/30th of the time step total. The time step total is calculated by multiplying the total event accumulated rainfall depth (defined in Section 2.3) by the proportion of rainfall assigned to that time step.

2.3.4 | Loss Removal

The Hec-Ras models applied here do not explicitly model urban drainage, infiltration or evapotranspiration. Instead, the rainfall reduction approach is used, whereby a net rainfall input, with losses already subtracted, is applied to the catchment. After accounting for losses, the depth of rainfall within all rainfall profiles is 14.44 mm in Lin Dyke and 20.10 mm in Wyke Beck. The rainfall reduction approach is standard practice in pluvial flood modelling and was applied in the national RoSWF map (Environment Agency 2019), amongst other surface water flood modelling studies (Chen et al. 2009; Chang et al. 2015; Henonin et al. 2013; Wang et al. 2023). We use ReFH2 software to remove losses in a spatially uniform manner. The mean summertime (June-July-August) daily rainfall for each catchment is specified as antecedent conditions for 15 days prior to the event. For Lin Dyke, this is 1.95 mm and for Wyke Beck, it is 2.02 mm. We calculate the antecedent conditions using the 1km CEH-GEAR-1 h gridded observations (Lewis et al. 2018) for the grid cells covering the catchment. Daily precipitation totals are calculated over the full period CEH-GEAR covers (1990–2014), and the mean values for each catchment are taken. The catchment locations are geographically close, and so the values are similar but not identical. After accounting for losses, the depth of rainfall within all rainfall profiles is 14.44 mm in Lin Dyke and 20.10 mm in Wyke Beck.

ReFH2 employs a soil moisture accounting method, where the rate of infiltration decreases throughout the rainfall event as the soil approaches saturation. Consequently, if the peak rainfall occurs later in the event, it experiences less attenuation (Figure 3b). In ReFH2, urban catchments are represented as a combination of pervious and impervious surfaces, with losses determined

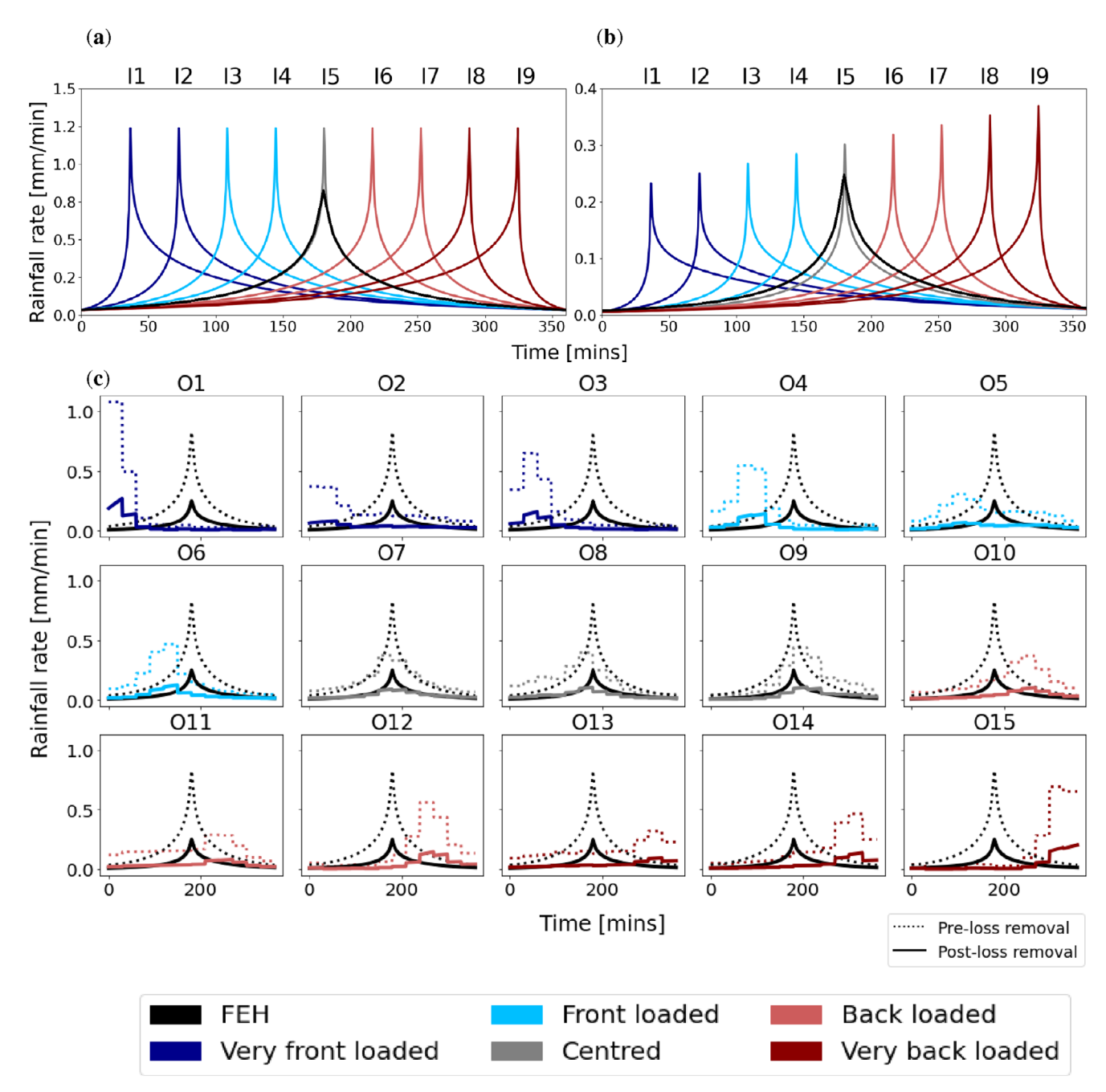


FIGURE 3 | Hyetograph profiles for a 6-h duration, 1-in-100 year return period event in the Lin Dyke catchment, including (a) idealised profiles, pre-loss removal, (b) idealised profiles, post-loss removal, and (c) observed profiles, pre and post-loss removal. The FEH summer profile is included in all plots in black. The profile classifications are explained further in Table 1.

 $\textbf{TABLE 1} \quad | \quad \text{Descriptions of idealised and observed profiles, and abbreviations used in text.}$

Title	Description	Idealised profiles	Observed profiles
Very front-loaded	Max intensity occurs in first 20% of storm duration	I1, I2	O1, O2, O3
Front-loaded	Max intensity occurs in second 20% of storm duration	I3, I4	O4, O5, O6
Centred	Max intensity occurs in middle 20% of storm duration	I5	O7, O8, O9
Back-loaded	Max intensity occurs in second last 20% of storm duration	I6, I7	O10, O11, O12
Very back-loaded	Max intensity occurs in last 20% of storm duration	18, 19	O13, O14, O15

by the proportion of the catchment identified as urban in the ReFH2 catchment descriptors. In contrast to RoFSW, we chose not to apply any losses to urban drainage systems. This decision is based on the understanding that our models encompass the entire catchment area, making it reasonable to assume that runoff entering the drainage system will ultimately flow into the river. While there may be timing limitations of surface water drainage return due to this assumption, it does ensure the total runoff volumes are representative for the whole catchment.

2.4 | Flood Classification

The maximum flood depth and velocity of flooding experienced in each cell across the whole model run time is exported from Hec-Ras for analysis. Only flood depths > 0.1 m are considered to constitute flooding, which is standard practice when assessing flood model results (e.g., Houston et al. (2011); Smith et al. (2019)). In our modelling results, we also aim to distinguish true flooding in areas which are usually dry, from areas of semipermanent water, which are designed to be, or are naturally, wet. We note that areas of permanent water, such as lakes or reservoirs, can appear as floodwaters in the results of Hec-Ras simulations due to how the software handles the interactions between river channels and adjacent floodplains. In Figure 4, areas which are classified in the land use data as fresh water are marked with hatching. This includes Waterloo Lake in the north of Wyke Beck catchment, and the substantial Fairburn Ings wetland region in the downstream area of Lin Dyke. In all of the analysis we exclude any areas identified as fresh water in the land use classification. Figure 4 also reveals that the fresh water land use class does not cover the whole wetland area in Lin Dyke—perhaps because the wetlands are somewhat ephemeral—and also fails to capture some other areas of permanent water, such as some fishing ponds to the south of Kippax. Considering this, Figure 4 also illustrates a boundary drawn for Lin Dyke which is used to additionally filter the results to ensure that none of these wetland areas are erroneously included in our results.

Our analysis includes calculation of the total flood affected area. This refers to the area in which flooding is experienced at some point during the model run time. Importantly, this whole area may not—and most likely will not—be all inundated at the same time. The next sections outline the approach taken to considering the flood depth, velocity and hazard categories of the flood waters.

2.4.1 | Flood Depth and Velocity Categories

The flooded depths and velocities are considered in reference to the categories displayed in Table 2. These have been defined by the Environment Agency (2019), based on feedback from local flood authorities undertaken as part of the creation of the RoFSW map.

2.4.2 | Hazard Classifications

The flood hazard rating (HR) is calculated using Equation (1) as a function of flood depth (D), velocity (V) and a debris factor (DF). The debris factor is set, irrespective of the land use type,

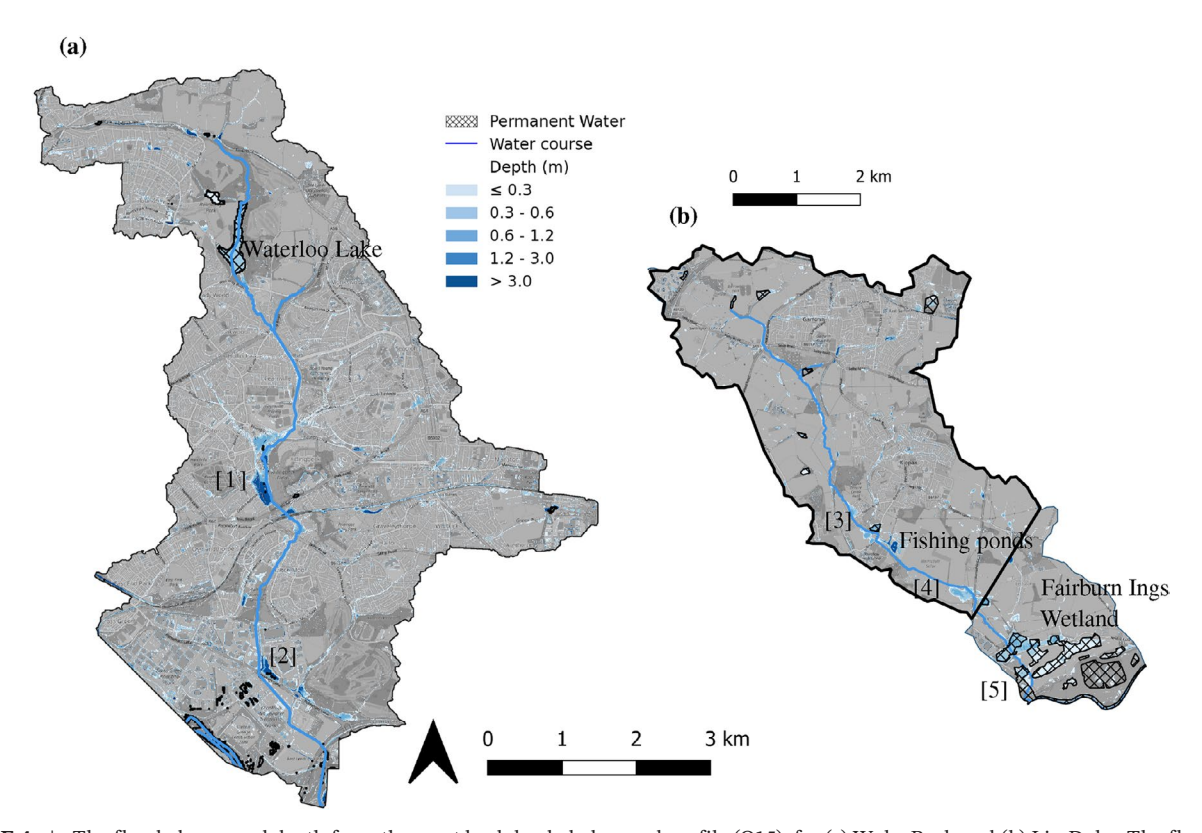


FIGURE 4 | The flooded area and depth from the most back-loaded observed profile (O15), for (a) Wyke Beck and (b) Lin Dyke. The flood depth categories correspond to those in Table 2. The watercourse is marked, and areas of permanent water according to the land cover classes in Section 2.1 are marked with hatching. Areas of interest are marked with numbers and discussed in the text.

TABLE 2 | Flood depth, velocity and hazard classifications (Environment Agency 2019).

Flood depth	Description				
< 0.1 m	Considered to pose minimal hazard				
0.1-0.3 m	Generally considered safe, likely to exceed kerb height				
0.3-0.6 m	Unsafe for small vehicles, likely to cause property damage				
0.6-1.2 m	Unsafe for all vehicles, and vulnerable groups, likely to cause property damage and exceed flood resilience measures level				
>1.2 m	Unsafe for vehicles and people, buildings are vulnerable to failure				
Flood velocity	Description				
$< 0.25 \mathrm{m s^{-1}}$	Considered essentially still				
$0.25 - 0.5 \mathrm{ms^{-1}}$	Generally considered safe, could be a hazard to vehicles and vulnerable groups at deep depths				
$0.50 - 2.0 \mathrm{m s^{-1}}$	Could be a hazard to vehicles and people at deep depths				

Hazard class	Hazard rating (HR)	Description
Low	<0.75	Very low hazard—caution
Moderate	0.75-1.25	Danger for some— includes children, the elderly and the infirm
Significant	1.25-2.0	Danger for most— includes the general public
Extreme	>2.0	Danger for all—includes the emergency services

as 0.5 for depths \leq 0.25 m, or 1 for depths > 0.25 m (Environment Agency 2019).

$$HR = D^*(V + 0.5) + DF$$
 (1)

Unsafe for vehicles and people,

buildings are vulnerable to failure

Table 2 provides thresholds for classifying this hazard rating according to the hazard it poses to people (Surendran et al. 2008).

3 | Results

 $> 2.0 \,\mathrm{m\,s^{-1}}$

3.1 | Overview of Catchment Flooding

To illustrate the areas of the catchment generally susceptible to flooding, the maximum flood depths associated with the most back-loaded observed profile (O15) leading to the most severe flooding are plotted in Figure 4a for Wyke Beck and Figure 4b for Lin Dyke. In both catchments, substantial inundated areas are observable around the track of the main watercourse. In Wyke Beck, the most notable areas are: in the centre of the catchment, to the east of Harehills district (Figure 4a-1); and around the industrial estate in the southern reaches of the catchment (Figure 4a-2). In Lin Dyke, prominent inundated areas include locations to the south of Kippax, where the watercourse intersects a main road (Figure 4b-3,4), and the area of wetlands in the lower catchment reaches (Figure 4b-5). We are primarily interested in urban areas, and in both catchments, flooding of streets and gardens are simulated by the model.

3.2 | Changes to Catchment Flooding

The following key differences in catchment flooding are observed:

- Back-loaded profiles result in more of the catchment experiencing flooding at some point during the simulation than front-loaded profiles.
- The majority of the cells which are flooded with the backloaded profile scenario, but not with the front-loaded profile scenario, are within the least severe depth and hazard classes, but in the higher velocity categories.
- Back-loaded profiles do not tend to cause new areas to flood, but incrementally increase flood extent in existing affected areas.
- Ack-loaded profiles reach their maximum flood extent later, and this extent is larger than for front-loaded profiles.

These results are explored in more detail in the sections below.

3.2.1 | Total Flood Extent

Our results demonstrate that rainfall events with the same total rainfall depth, but distributed differently over time, can result in different flood extents. With the idealised profiles, the most back-loaded profile (I9) causes the most extensive flooding in both catchments (Figure 5a,c), with ~15% greater flooded area than the most front-loaded profile (I1). Similarly, for the observed profiles, the most back-loaded profile (O15) results in the most extensive flooding in both catchments (Figure 5b,d), with ~25% greater flooded area than the frontloaded profile with the least extensive flooding (O2). For the idealised profiles, as the timing of the peak is shifted towards the end of the profile there is a consistent trend towards more extensive flooding. However, for the observed profiles, the trend is noisier. For instance, there are front-loaded profiles (e.g., O1) with greater flooded areas than back-loaded profiles (e.g., O10). This can be attributed to the concurrent variation in peak intensity found in the observed profiles. The frontloaded profile O1 has a much higher peak intensity than the back-loaded profile O10, and this also influences the flooding generated. Given these findings, in subsequent comparisons, we focus on I1 (the most front-loaded) and I9 (the most backloaded) for the idealised profiles. For the observed profiles, we compare O2 (the second most front-loaded, but which results

in the least flooding due to its low peak) and O15 (the most back-loaded). We also note that the centred observed profiles result in a smaller flooded area than the FEH profile, likely because of the observed profiles' lower peak magnitudes (see Figure 3d).

Figure 5e-h considers only flooding in areas which are classed as urban or semi-urban, as defined in the land cover classes described in Section 2.2. We include this additional breakdown of results to rule out the possibility that the difference between the profiles is confined only to more rural parts of the catchment (e.g., fields) where flooding is less consequential. This demonstrates that, to the contrary, the differences between the sets of profiles are at least as large (or larger) for the urban areas than for the whole catchment.

3.2.2 | Flood Severity

There is limited evidence that the temporal distribution of rainfall within storm events affects the severity of the resulting flooding. The most notable changes occur to the flood water velocities.

3.2.2.1 | **Depth.** All rainfall profiles result in flood events with a similar proportion of maximum depths across the categories in Table 2. Table 3 shows that for both catchments and profile types, just over half of the maximum flood depths fall between 0.1 and 0.3 m, with progressively smaller proportions occurring in the deeper categories. Across all profiles and catchments, the front-loaded profiles are associated with slightly lower proportions of flooding in the shallowest category compared to the most back-loaded profiles, and slightly higher proportions

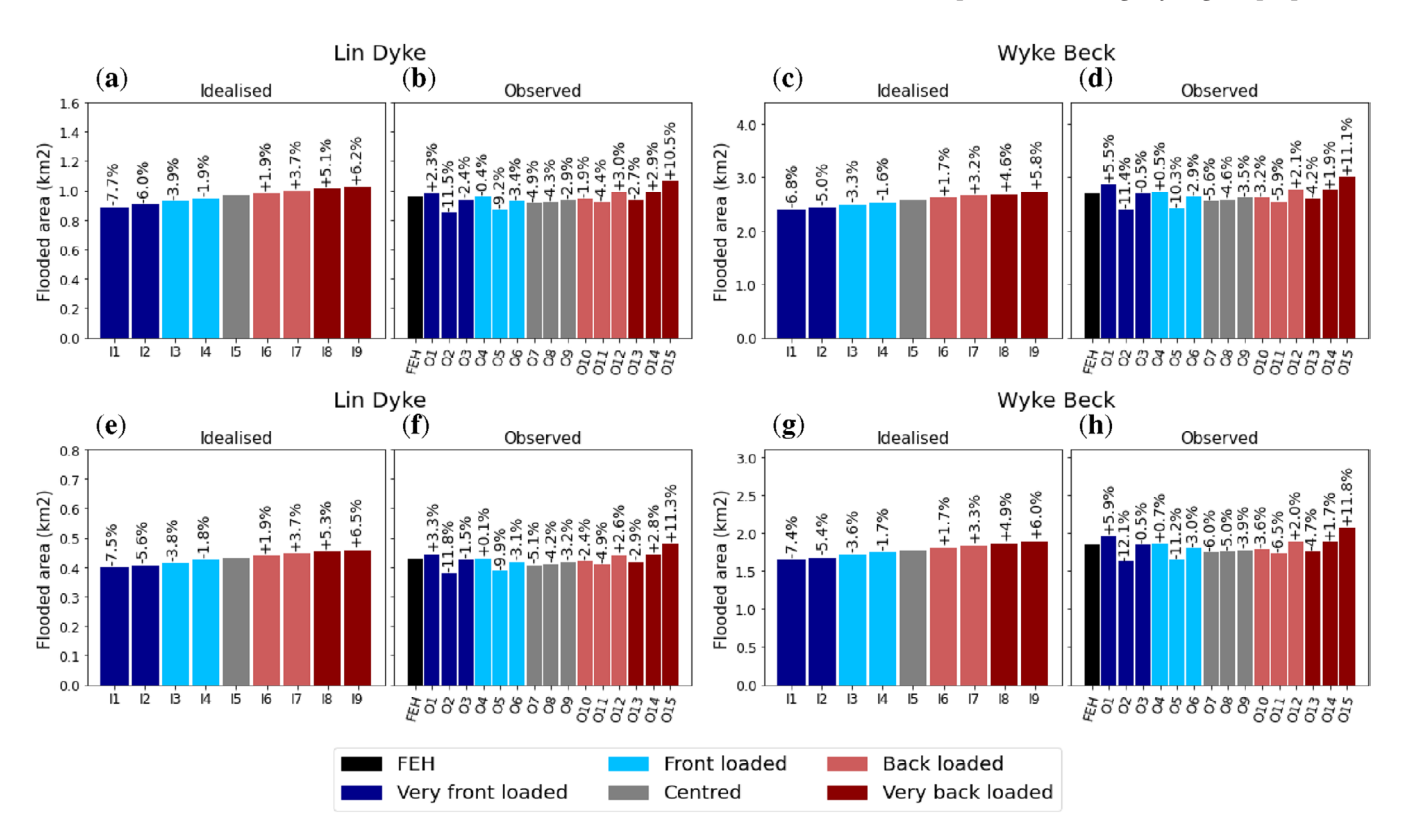


FIGURE 5 | The total area flooded (>0.1 m flood depth) at any point during the simulation, for (a–d) areas which are not permanent water and (e–h) for urban areas. The percentage differences are shown relative to the centred profile (I5) for the idealised profile and relative to the FEH profile for the observed profiles.

TABLE 3 | The proportion of the total flooded area with maximum flood depth in each of the depth categories from Table 2 for the most front-loaded (I1 and O2) and most back-loaded (I9 and O15) idealised and observed profiles.

	Idealised				Obser	ved			
	Lin Dyke		Wyke Beck		Lin Dyke		Wyke Beck		
	I1	I9	I1	I 9	O2	015	02	015	
Total flooded area (km²)	0.89	1.03	2.40	2.72	0.85	1.07	2.40	3.01	
0.1-0.3 m	51%	52%	56%	58%	50%	52%	56%	59%	
0.3-0.6 m	29%	26%	22%	21%	29%	26%	22%	21%	
0.6-1.2 m	16%	16%	14%	13%	15%	16%	14%	12%	
>1.2 m	6%	6%	8%	8%	6%	6%	8%	7%	

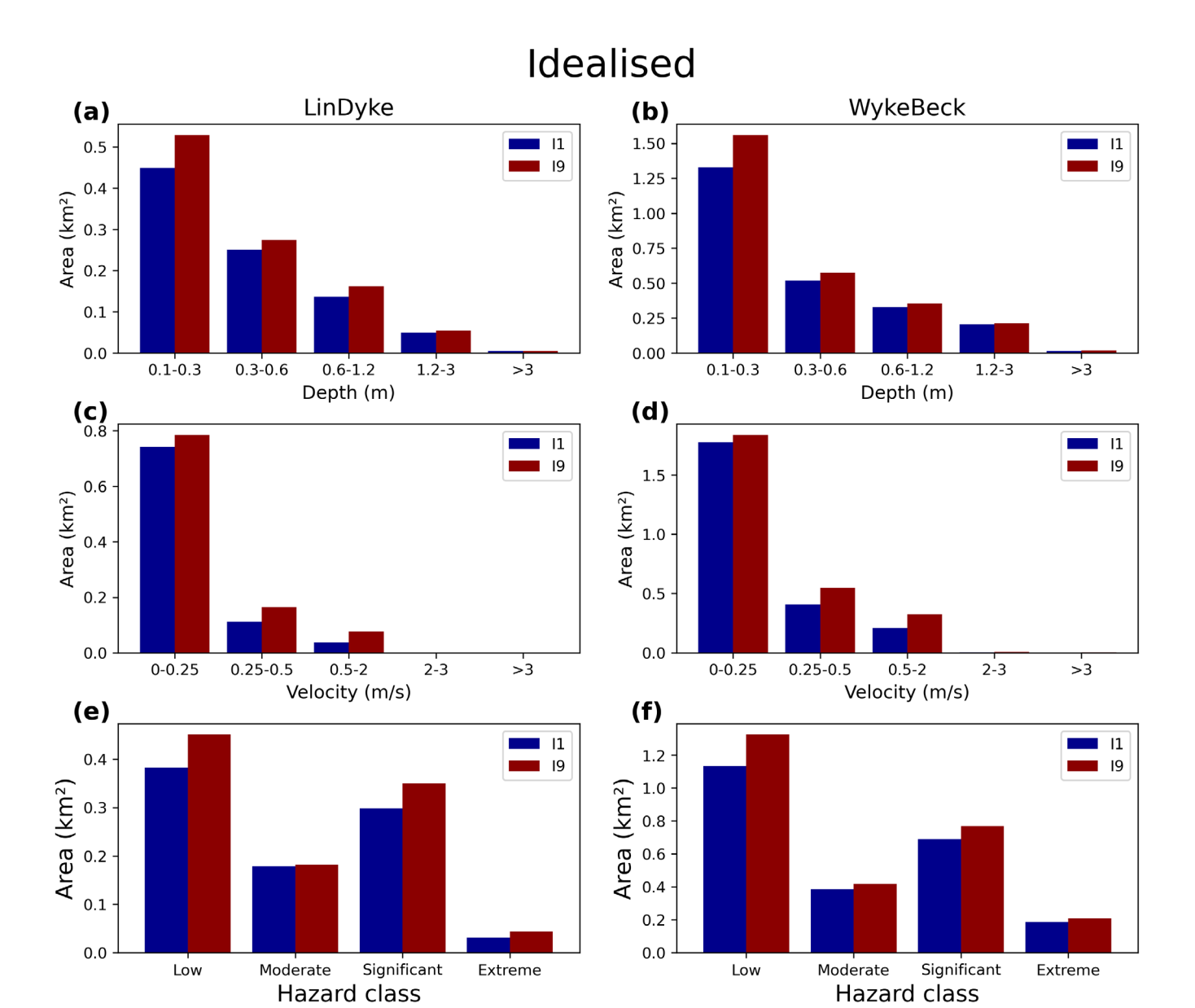


FIGURE 6 | The area in each of the depth, velocity and hazard classes defined in Section 2.4 including (a–f) for idealised profiles and (g–I) for observed profiles. In each case, the most front-loaded (I1 and O2) and most back-loaded profiles (I9 and O15) are plotted.

in the more severe depth ranges of 0.3-0.6 m and 0.6-1.2 m, although the differences are small.

Nevertheless, the larger overall extent of flooding with the back-loaded profile means that, despite the relative proportions of flooding across depth categories remaining the same, the absolute areas in all, including the most severe, depth categories are still greater. Figure 6a,b,e,f show this increase in absolute area, including for depths between 0.3 and 0.6m (which begin to threaten cars and properties), 0.6 and 1.2m (where damage to these becomes more likely), and depths greater than 1.2m (considered unsafe for all people and vehicles). The bulk of the extra flooding has maximum depths between 0.1 and 0.3 m. We note that while these depths are generally not considered highly dangerous, they can still cause significant nuisance. For example, water around 15cm deep can reach the underbody of a car and stall it (Pregnolato et al. 2017), and depths over 10cm (the standard kerb height) can begin to cause property damage (Moftakhari et al. 2018).

In summary, while the relative distribution of flood depths remains largely unchanged, the greater absolute area of severe flooding suggests that back-loaded profiles can lead to more severe impacts, affecting more properties and potentially causing greater damage.

3.2.2.2 | **Velocity.** Table 4 shows that the flood events modelled here are predominantly composed of floodwaters moving at velocities of less than $0.25\,\mathrm{m\,s^{-1}}$. The table also highlights that the timing of the rainfall peak influences the distribution of floodwaters across different velocity categories. Specifically, back-loaded rainfall profiles result in a higher proportion of flooding in the faster velocity categories from Table 2 and a smaller proportion of flooding in the slower velocity categories compared to front-loaded profiles.

Furthermore, Figure 6c,d,g,h illustrate that the absolute increase in flooded area for back-loaded profiles is greater in the

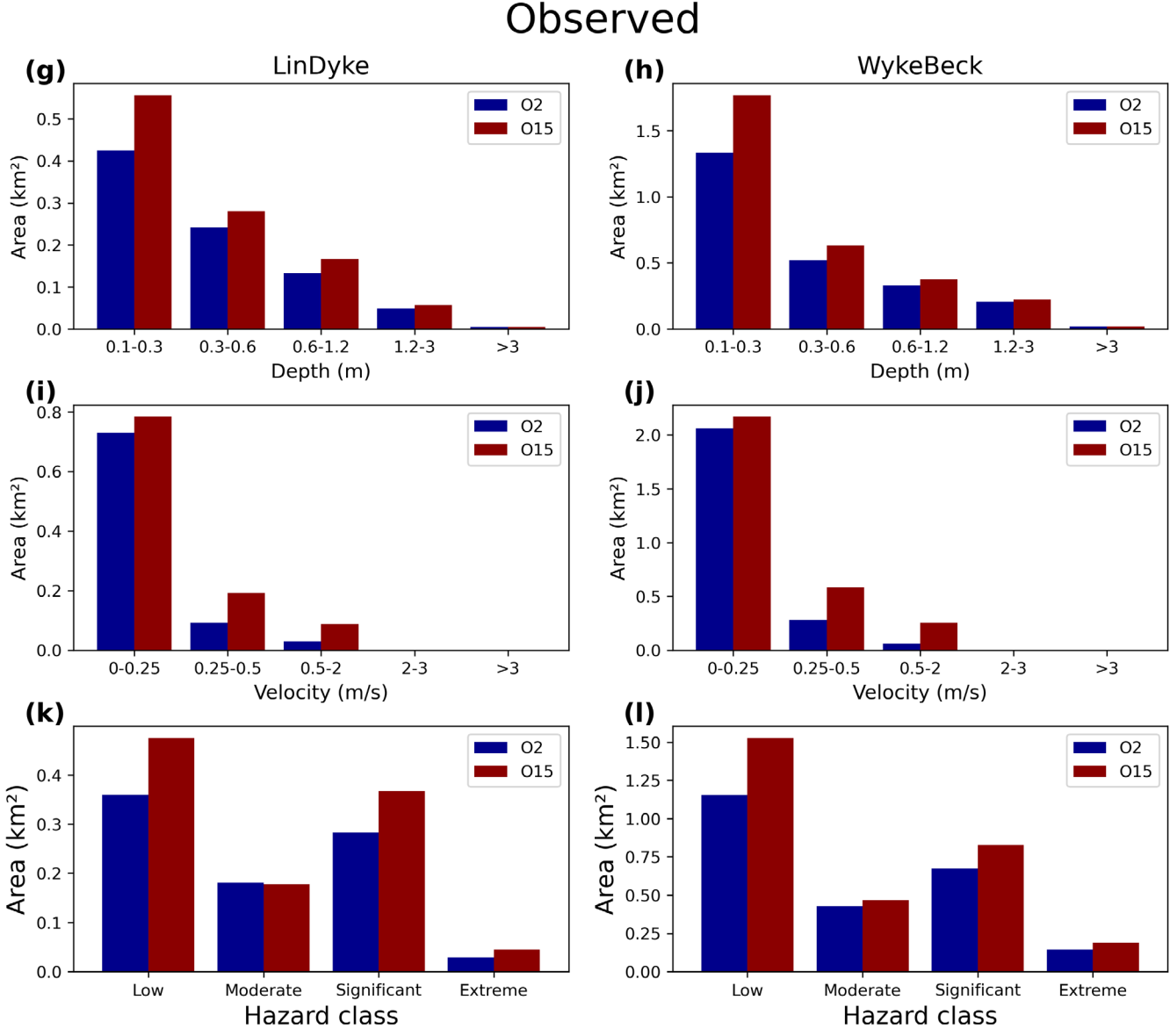


FIGURE 6 | (Continued)

higher velocity ranges $(0.25-0.50\,\mathrm{m\,s^{-1}}$ and $0.5-2.0\,\mathrm{m\,s^{-1}})$ than in the slowest velocity category.

3.2.2.3 | **Hazard.** Hazard class is a composite measure combining flood depth, velocity and a debris factor, with this debris factor relating to land use (see Section 2.4.2). In accordance with the results for depth and velocity, Figure 6 illustrates that the absolute increase in flood-affected area in the back-loaded profiles occurs predominantly in the low hazard class across both catchments and sets of profiles. There is a smaller, but still notable, increase in the absolute area in the significant hazard class, and an even smaller increase in the extreme category.

3.2.3 | Spatial Changes to the Flood Extent and Depth

Figure 7 illustrates, for each cell in the model domain for both catchments, the idealised rainfall profile which results in the deepest (a, c) and fastest moving (b, d) flood waters. This

highlights that the increased severity of flooding found with more back-loaded profiles is generally consistent at locations across the catchment.

Section 3.2.1 establishes that the most back-loaded rainfall profile leads to the most extensive flooding. Visual analysis of the flood maps indicates that this additional flooding primarily results from incremental increases in areas that were already flooded in the more front-loaded profiles, rather than substantially affecting previously dry areas.

An illustrative example of the areas which are subject to the largest changes in the maximum depth values between the most front-loaded and back-loaded observed profiles is given in Figure 8 for Lin Dyke. The observed profiles are chosen for this demonstration because they exhibit the greatest difference in flood extent between the two extremes. In the vast majority of the catchment, the back-loaded profile experiences deeper maximum flood depths than the front-loaded profile. The deeper flooding

TABLE 4 | The proportion of the total flooded area with maximum flood velocities in each of the velocity categories from Table 2 for the most front-loaded (I1 and O2) and most back-loaded (I9 and O15) idealised and observed profiles.

	Idealised				Obser	served			
	Lin Dyke		Wyke Beck		Lin Dyke		Wyke Beck		
	I1	I9	I1	I9	O2	015	02	015	
Total flooded area (km²)	0.89	1.03	2.40	2.72	0.85	1.07	2.40	3.01	
$0.0 - 0.25\mathrm{ms^{-1}}$	83%	76%	74%	68%	86%	74%	86%	72%	
$0.25 - 0.5 \mathrm{ms^{-1}}$	12%	16%	17%	20%	11%	18%	12%	20%	
$0.5 - 2.0 \mathrm{ms^{-1}}$	4%	8%	9%	12%	4%	8%	2%	9%	
$> 2.0 \mathrm{ms^{-1}}$	0%	0%	0%	0%	0%	0%	0%	0%	

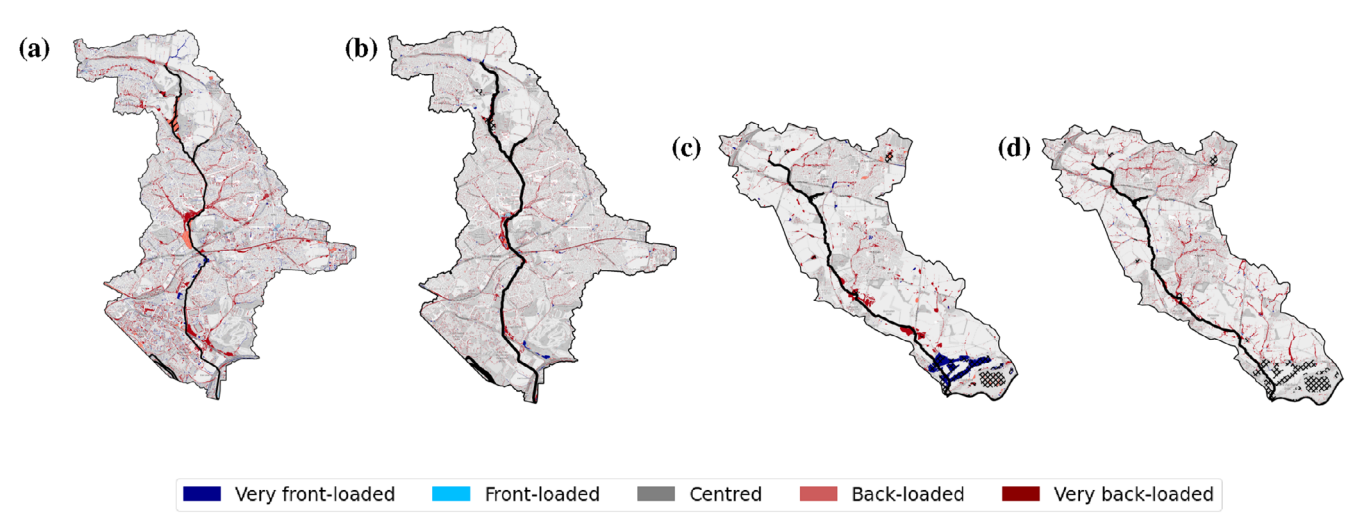


FIGURE 7 | Rainfall profiles associated with the deepest (a, c) and fastest (b, d) flooding for Wyke Beck (a, b) and Lin Dyke (c, d) with the idealised profile scenarios.

associated with the front-loaded profile in the bottom area of wetlands (Figure 8a-1) is likely an artefact of the duration of the model run time. Even after 3 days, the model has not reached a steady state, and water is still moving through the catchment. Consequently, for the back-loaded profile, where the rainfall arrives later, the depths in these storage areas in the lower reaches of the catchment are yet to reach the same levels as they do with the front-loaded profile. Given more time, we assume the depths in these areas would also be higher in the back-loaded profiles.

The back-loaded profile has the most substantial depth increases over the most front-loaded profile in the areas marked on the plot in Figure 8. The first of these locations (Figure 8a-2) is the fishing ponds marked in Figure 4. The latter two (Figure 8a-3,4) are inundated areas which form at junctions between a major road and the watercourse. Notably, these ponds develop over fields and therefore have less serious consequences. A more detailed look at the urban areas is provided for both Kippax (Figure 8b) and Garforth (Figure 8c), as well as an even more detailed look at the north-west of Garforth (Figure 8d). This shows that increases in flood depths of between 5 and 20 cm are also commonly experienced in the urban areas which are vulnerable to flooding. These are not negligible increases, and could make the difference between

floods over-topping the kerb (which is usually around 10 cm high) to cause property damage.

3.2.4 | Simultaneously Flooded Extent Over Time

The previous sections report the maximum flood depth, velocity, and hazard found during the whole simulation period. Whilst this analysis offers a snapshot of the worst-case scenario for peak flood risk, it does not capture how flooding evolves over time. In this section, we explore this further.

For idealised rainfall, the most front-loaded profile reaches its maximum flooded extent 120 (130) minutes earlier in Lin Dyke (Wyke Beck) than the most back-loaded profile (Figure 9a,c). The timing difference in peak rainfall intensity between these two profiles is 288 min in both catchments (Figure 3b). In agreement with the worst-case values in Figure 5, in Lin Dyke (Wyke Beck) the maximum simultaneously flooded area for the most front-loaded profile is only 91% (84%) that of the most back-loaded profile.

For observed rainfall profiles, the maximum simultaneously flooded area for the front-loaded profile is 89% (86%) the size of the back-loaded profile (Figure 9b,d). The timing difference is

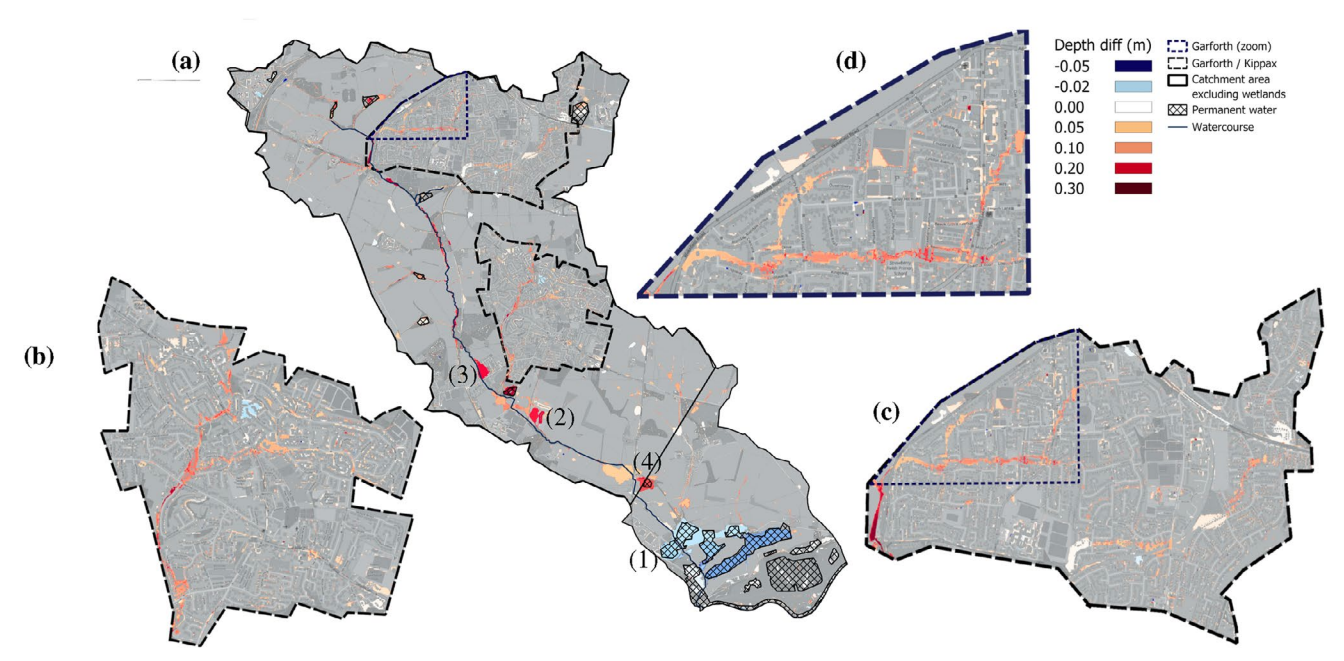


FIGURE 8 | The difference in maximum flood depth between most front-loaded (O2) and most back-loaded (O15) observed profiles, across (a) the whole of Lin Dyke, (b) the Kippax urban area, (c) the Garforth urban area, and (d) a small section of Garforth. Areas of interest are marked with numbers and discussed in the text.

even greater, with the front-loaded profile reaching its peak extent 250 (300) minutes earlier in Lin Dyke (Wyke Beck) (Figure 9b,d). This is likely due to the timing of the peak in rainfall intensity between the most front-loaded and most back-loaded profiles being even greater for the observed profiles at 331 min (Figure 3c).

It is worth noting that the levelling off in the flooded area after around ~800 min which we see in Figure 9 is to be expected. In pluvial flood modelling the focus is on accurately capturing the peak flood extent, which is predominantly what determines the flood risk. Capturing how the flood waters recede would require significantly more advanced representation of the hydrological processes governing the movement, distribution and properties of water over time. A lack of model connectivity prevents water draining and causes it to remain ponded in an unrealistic manner. However, modelling the hydrology of drainage more precisely would require extra—often difficult to access—data and come at a higher computational cost. Considering the limited benefits in terms of capturing the most relevant impacts of pluvial flooding, these costs are generally not deemed worthwhile.

4 | Discussion and Conclusions

Storms are inherently unique phenomena characterised by a multitude of variables such as accumulated rainfall depth, duration, intensity, temporal and spatial patterns and antecedent wetness conditions (Loveridge and Rahman 2018). Attempting to represent the infinite range of possibilities associated with these variables in flood modelling would pose insurmountable computational challenges. Therefore, the design storm approach serves as a pragmatic solution, simplifying the modelling process to make it computationally feasible and readily reproducible. Here we use a simulation model, specifically a hydraulic rain-on-grid model, following Beven (1989), to explore

the implications for pluvial flood modelling of the assumptions made in simplified design storms about the temporal structure of rainfall in real events.

Our experiments with idealised profiles show a demonstrable link between the timing of peak rainfall intensity and the flood extent and severity. There is a systematic increase in the total floodaffected area as the peak moves towards the end of the event, with approximately a 15% increase with the most back-loaded profile compared to the most front-loaded. This could be attributable to several factors: Firstly, the prolonged period of light rainfall preceding the peak in back-loaded profiles may fill up small-scale storage elements within the landscape, such as small topographic depressions (e.g., puddles) or small drainage channels and roadside gutters (Bulti and Abebe 2020). Consequently, when the more intense rainfall arrives, there is less storage available, so water concentrates more quickly, and levels of surface runoff may be higher. Furthermore, the cumulative effect of runoff from earlier stages of the event, coupled with the intensifying rainfall towards the end, can lead to a compounding effect, where floodwaters continue to rise, spreading over larger regions.

Idealised profiles, while useful for isolating the effect of peak timing by keeping peak intensities constant, lack physical realism. For instance, Villalobos Herrera, Blenkinsop, Guerreiro, and Fowler (2023) showed that the highest peak intensities typically occur only in very front-loaded or very back-loaded events. By testing with the 15 observed profiles, in which the timing and magnitude of peak intensity covary, we thereby capture a more representative range of flood response expected with realistic combinations of these parameters. Notably, the most front-loaded profile still results in the smallest flood-affected area, while the most back-loaded profile leads to the largest. In this case, the difference between these profiles is even greater, reaching 25%. The relationship between the timing of peak intensity

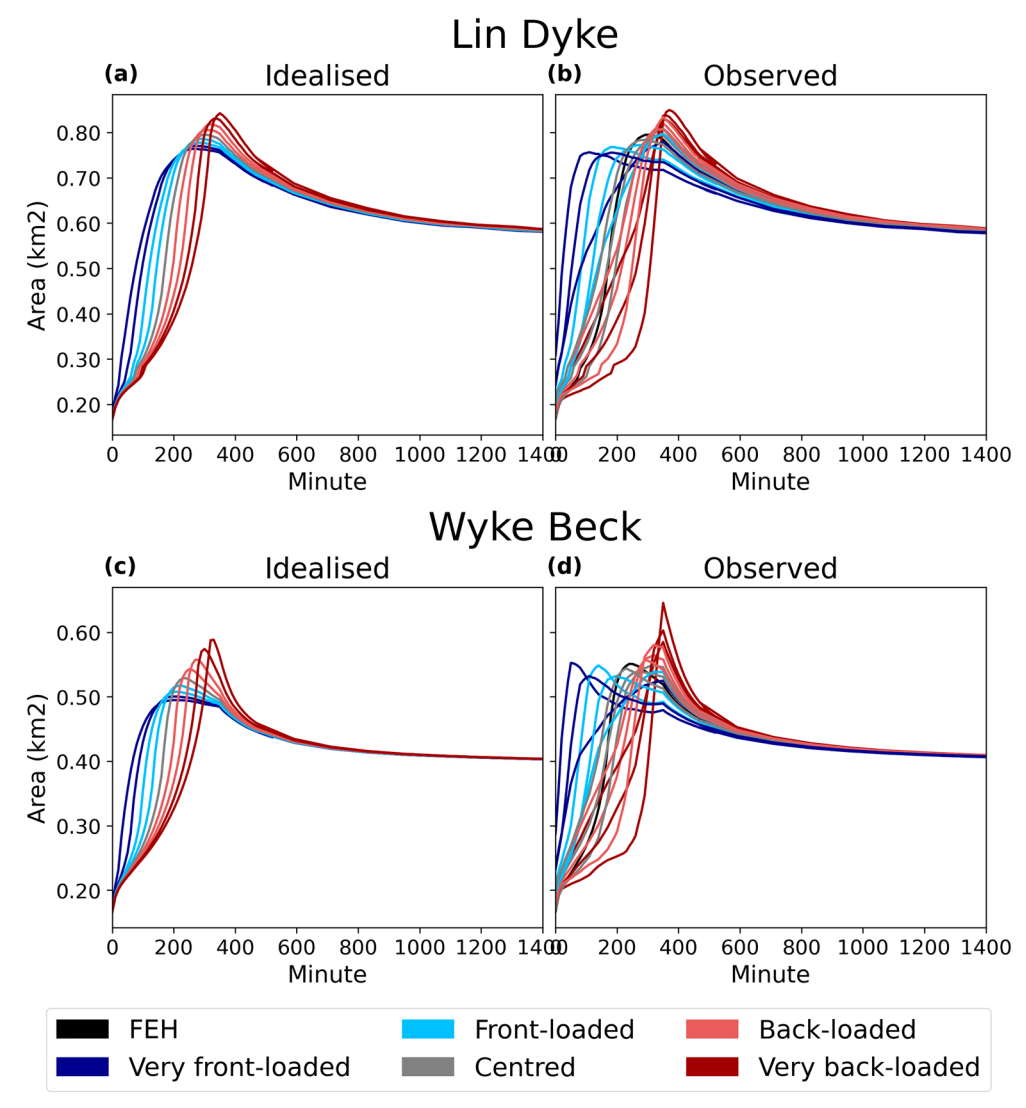


FIGURE 9 | The simultaneously flooded extent, plotted every 10 min for the first 8 h and every 2 h for the remainder of the model run time. For (a) Lin Dyke catchment, idealised profiles, (b) Lin Dyke catchment, observed profiles; and (c) Wyke Beck catchment, idealised profiles, (d) Wyke Beck catchment, observed profiles. The plots are cut off after 1400 min (~1 day) to allow the differences earlier in the process to be more clearly inspected.

and flood extent and severity, however, is less consistent than with the idealised profiles. For instance, while the peak arrives later in profile O7 than in profile O5, O5 also has a higher peak intensity and is associated with a much larger flooded extent.

The modelling approach used here has some limitations. Standard pluvial flood hazard assessment methodologies are used, which apply a rainfall removal rate to represent the drainage capacity and infiltration. This simplified approach assumes that infiltration and the influence of antecedent conditions will occur in a spatially uniform manner. We propose that the disparity between the more pronounced flooding observed with the back-loaded profile and the milder flooding associated with the front-loaded profile could be even larger if the impacts of variations in permeable ground saturation and the filling of urban drainage systems during the early stages of the event were incorporated (Houston et al. 2011).

The primary objective of this study is to examine the implications of simplifying the representation of the time-varying distribution of rainfall in design storms. The selected catchments are utilised not for the purpose of evaluating specific outcomes in these areas, but rather as tools to fulfil this objective. Catchment characteristics, particularly in complex urban watersheds, play an important role in shaping hydrological responses (Singh 1997; Szeląg et al. 2022; Ten Veldhuis et al. 2018). Therefore, the unique attributes of the catchments used in this study, for example, shape, slope, topography, size, orientation, urbanisation, and so forth, influence the extent to which they respond to the different rainfall profiles. This research presents an indicative example of the range of responses possible in a catchment purely from variations in rainfall temporal distribution, but the responses found here may not be representative of all catchments. Understanding of the interplay between catchment characteristics and rainfall variability is currently limited (Ten Veldhuis et al. 2018), and we support the need for more research into these complex relationships. Even with further research, it is unlikely that a universal relationship between temporal rainfall variability and catchment characteristics will be uncovered.

Applying a single storm framework has evident shortcomings. The FEH profile, like other hyetographs, focuses on

representing the average characteristics of rainstorms. However, as Villalobos Herrera, Blenkinsop, Guerreiro, Dale, et al. (2023) highlight, there is no true concept of an 'average' storm, and indeed averaging across storms masks critical variability that we have shown influences flood hazard. Our results indicate that the flood affected area predicted by the FEH profile can differ by approximately 10% from those generated by more realistic frontand back-loaded rainfall events. Moreover, the FEH profile does not even sit near the middle of the observed profile results, predicting a greater flood extent than 60% of observed profiles in Wyke Beck and 73% in Lin Dyke. We hypothesise that this discrepancy arises from the nonphysical combination of a central, highly intense rainfall peak in the FEH profile. If a single storm framework must be used, we recommend selecting from the profiles derived by Villalobos Herrera, Blenkinsop, Guerreiro, and Fowler (2023), tailored to storm duration, to improve result accuracy. For instance, front-loaded profiles have been shown to be most common for very short-duration storms.

Ideally, alternative approaches to a single-storm framework should be considered, such as ensemble modelling or Monte Carlo simulations (Nathan et al. 2003). Villalobos Herrera, Blenkinsop, Guerreiro, Dale, et al. (2023) illustrate an evidencebased approach to deriving a suite of profiles, varying at different durations, which could replace the FEH profile. Similar to the work presented here, ensemble modelling involves running a model multiple times using an ensemble of rainfall events (on the order of 10-100 events) with variations to the rainfall temporal pattern, and all other characteristics held constant (Loveridge and Rahman 2018). This approach is less complex than a full Monte Carlo simulation, where all variables deemed crucial for flooding are allowed to vary (e.g., duration, rainfall depth, initial losses, temporal pattern). In a Monte Carlo simulation, values for these variables are randomly sampled from probability distributions or sets of values, enabling consideration of the joint probability of all factors which contribute to flooding (Ball et al. 2019). An excellent example of the ensemble approach is found in the Australian Rainfall and Runoff (ARR) national guidance document for estimation of design floods in Australia (Ball et al. 2019). In its most recent update the ARR recommends, instead of the previous single storm method, to use an ensemble of temporal patterns derived from extensive data and specific to location, duration and frequency. There are 10 temporal patterns for each duration, ranging from 10 min to 7 days, for each of four return period bands and each of 12 regions. Consequently, flood modelling outcomes are more tailored to the specific characteristics of the rainstorm and region, while also providing a range or ensemble of potential forecast outcomes in order to better quantify forecast uncertainty. Villalobos Herrera, Blenkinsop, Guerreiro, and Fowler (2023)'s profiles offer an opportunity to move towards a similar system in the UK, and we recommend exploring how to implement this effectively.

Data Availability Statement

The data that support the findings of this study are available at https://zenodo.org/records/10573453. The data used in the modelling were derived from the following resources available in the public domain: [FEH web service: https://fehweb.ceh.ac.uk/; CEH Land Cover Map 2020 https://catalogue.ceh.ac.uk/documents/14a9ec05-071a-43a5-a142-e6894f3d6f9d; Environment Agency LIDAR composite DTM at 1m/2m

for Lin Dyke/Wyke Beck https://www.data.gov.uk/dataset/67639c1b-ac0e-492a-abba-02ed436f826f/lidar-composite-dtm-2019-2m].

References

Archer, D. R., and H. J. Fowler. 2018. "Characterising Flash Flood Response to Intense Rainfall and Impacts Using Historical Information and Gauged Data in Britain." *Journal of Flood Risk Management* 11: \$121–\$133

Balbastre-Soldevila, R., R. García-Bartual, and I. Andrés-Doménech. 2019. "A Comparison of Design Storms for Urban Drainage System Applications." *Water* 11, no. 4: 757.

Ball, J., M. Babister, R. Nathan, et al. 2019. *Australian Rainfall and Runoff – A Guide to Flood Estimation*. Geosceience Australia.

Beadle, M. 2021. "Identifying the Impact of Climate Change on the Pluvial Flood Hazard in Leeds" (Master's thesis).

Berne, A., and W. F. Krajewski. 2013. "Radar for Hydrology: Unfulfilled Promise or Unrecognized Potential?" *Advances in Water Resources* 51: 357–366

Beven, K. 1989. "Changing Ideas in Hydrology the Case of Physically-Based Models." *Journal of Hydrology* 105, no. 1–2: 157–172.

Bruni, G., R. Reinoso, N. Van De Giesen, F. Clemens, and J. Ten Veldhuis. 2015. "On the Sensitivity of Urban Hydrodynamic Modelling to Rainfall Spatial and Temporal Resolution." *Hydrology and Earth System Sciences* 19, no. 2: 691–709.

Brunner, G. W. 2016. HEC-RAS River Analysis System: Hydraulic Reference Manual, Version 5.0, 547. US Army Corps of Engineers-Hydrologic Engineering Center.

Bulti, D. T., and B. G. Abebe. 2020. "A Review of Flood Modeling Methods for Urban Pluvial Flood Application." *Modeling Earth Systems and Environment* 6: 1293–1302.

Butler, D., and J. Davies. 2004. *Urban Drainage*. Second ed. CRC Press

Chang, T.-J., C.-H. Wang, and A. S. Chen. 2015. "A Novel Approach to Model Dynamic Flow Interactions Between Storm Sewer System and Overland Surface for Different Land Covers in Urban Areas." *Journal of Hydrology* 524: 662–679.

Chen, A. S., S. Djordjevic, H. J. Fowler, et al. 2009. "Pluvial Flood Modelling of the South East London Resilience Zone in the Community Resilience to Extreme Weather (CREW) Project." In Proceedings of the Flood and Coastal Risk Management Conference. Telford, Uk. CIWEM.

Costabile, P., C. Costanzo, D. Ferraro, and P. Barca. 2021. "Is HEC-RAS 2D Accurate Enough for Storm-Event Hazard Assessment? Lessons Learnt From a Benchmarking Study Based on Rain-On-Grid Modelling." *Journal of Hydrology* 603: 126962.

Costabile, P., C. Costanzo, and F. Macchione. 2017. "Per-Formances and Limitations of the Diffusive Approximation of the 2-d Shallow Water Equations for Flood Simulation in Urban and Rural Areas." *Applied Numerical Mathematics* 116: 141–156.

Courant, R., K. Friedrichs, and H. Lewy. 1967. "On the Partial Difference Equations of Mathematical Physics." *IBM Journal of Research and Development* 11, no. 2: 215–234.

Davies, P., and L. Hancock. 2015. "How Critical Is Critical Duration in a 2D Surface Water Model?"

Dawdy, D., and J. M. Bergmann. 1969. "Effect of Rainfall Variability on Streamflow Simulation." *Water Resources Research* 5, no. 5: 958–966.

Einfalt, T., K. Arnbjerg-Nielsen, C. Golz, et al. 2004. "Towards a Roadmap for Use of Radar Rainfall Data in Urban Drainage." *Journal of Hydrology* 299, no. 3–4: 186–202.

Environment Agency. 2019. "What Is the Risk of Flooding From Surface Water Map?" https://assets.publishing.service.gov.uk/media/5db6ded540f0b6379a7acbb8/What-is-the-Risk-of-Flooding-from-Surface-Water-Map.pdf.

Environment Agency. 2021. "Flood and Coastal Erosion Risk Management Report: 1 April 2020 to 31 March 2021." https://www.gov.uk/government/publications/flood-and-coastal-risk-management-national-report/flood-and-coastal-erosion-risk-management-report-1-april-2020-to-31-march-2021.

Faulkner, D. 1999. Flood Estimation Handbook: Volume 2: Rainfall Frequency Estimation. Centre for Ecology & Hydrology.

Gabellani, S., G. Boni, L. Ferraris, J. Von Hardenberg, and A. Provenzale. 2007. "Propagation of Uncertainty From Rainfall to Runoff: A Case Study With a Stochastic Rainfall Generator." *Advances in Water Resources* 30, no. 10: 2061–2071.

Henonin, J., B. Russo, O. Mark, and P. Gourbesville. 2013. "Real-Time Urban Flood Forecasting and Modelling–a State of the Art." *Journal of Hydroinformatics* 15, no. 3: 717–736.

Hettiarachchi, S., C. Wasko, and A. Sharma. 2018. "In1018 Crease in Flood Risk Resulting From Climate Change in a Developed Urban Watershed-the Role of Storm Temporal Patterns." *Hydrology and Earth System Sciences* 22, no. 3: 2041–2056.

Houston, D., A. Werritty, D. Bassett, A. Geddes, A. Hoolachan, and M. McMillan. 2011. *Pluvial (Rain-Related) Flooding in Urban Areas: The Invisible Hazard*. Joseph Rowntree Foundation. http://www.jrf.org.uk/sites/files/jrf/urban-flood-risk-full.pdf.

Jenkins, K., J. Hall, V. Glenis, and C. Kilsby. 2018. "A Probabilistic Analysis of Surface Water Flood Risk in London." *Risk Analysis* 38, no. 6: 1169–1182.

Keifer, C. J., and H. H. Chu. 1957. "Synthetic Storm Pattern for Drainage Design." *Journal of the Hydraulics Division* 83, no. 4: 1332.

Kjeldsen, T. R. 2007. The Revitalised FSR/FEH Rainfall Runoff Method. NERC/Centre for Ecology & Hydrology.

Krvavica, N., and J. Rubinic´. 2020. "Evaluation of Design Storms and Critical Rainfall Durations for Flood Prediction in Partially Urbanized Catchments." *Water (Basel)* 12, no. 7: 2044.

Lambourne, J., and D. Stephenson. 1987. "Model Study of the Effect of Temporal Storm Distributions on Peak Discharges and Volumes." *Hydrological Sciences Journal* 32, no. 2: 215–226.

Lewis, E., N. Quinn, S. Blenkinsop, et al. 2018. "A Rule Based Quality Control Method for Hourly Rainfall Data and a 1 Km Resolution Gridded Hourly Rainfall Dataset for Great Britain: CEH-GEAR1hr." *Journal of Hydrology* 564: 930–943.

Li, T., G. Lee, and G. Kim. 2021. "Case Study of Urban Flood Inundation-Impact of Temporal Variability in Rainfall Events." *Water* 13, no. 23: 3438.

Loveridge, M., and A. Rahman. 2018. "Monte Carlo Simulation for Design Flood Estimation: A Review of Australian Practice." *Australasian Journal of Water Resources* 22, no. 1: 52–70.

Marsalek, J., and W. Watt. 1984. "Design Storms for Urban Drainage Design." *Canadian Journal of Civil Engineering* 11, no. 3: 574–584.

Moftakhari, H. R., A. AghaKouchak, B. F. Sanders, M. Allaire, and R. A. Matthew. 2018. "What Is Nuisance Flooding? Defining and Monitoring an Emerging Challenge." *Water Resources Research* 54, no. 7: 4218–4227.

Morton, R. D., C. G. Marston, A. W. O'Neil, and C. S. Rowland. 2020. "Land Cover Map 2017 (25m Rasterised Land Parcels, GB) [Data Set]." NERC Environmental Information Data Centre. https://doi.org/10.5285/499212CD-D64A-43BA-B801-95402E4D4098.

Nathan, R., E. Weinmann, and P. Hill. 2003. "Use of Monte Carlo Simulation to Estimate the Expected Probability of Large to Extreme Floods." In *International Hydrology and Water Resources Symposium*, 1–105. NSW.

Nguyen, V.-T.-V., N. Peyron, and G. Rivard. 2002. "Rainfall Temporal Patterns for Urban Drainage Design in Southern Quebec." In *Global Solutions for Urban Drainage*, 1–16.

Ochoa-Rodriguez, S., L.-P. Wang, A. Gires, et al. 2015. "Impact of Spatial and Temporal Resolution of Rainfall Inputs on Urban Hydrodynamic Modelling Outputs: A Multi-Catchment Investigation." *Journal of Hydrology* 531: 389–407.

Paschalis, A., S. Fatichi, P. Molnar, S. Rimkus, and P. Burlando. 2014. "On the Effects of Small Scale Space–Time Variability of Rainfall on Basin Flood Response." *Journal of Hydrology* 514: 313–327.

Peleg, N., F. Blumensaat, P. Molnar, S. Fatichi, and P. Burlando. 2017. "Partitioning Spatial and Temporal Rainfall Variability in Urban Drainage Modelling." *Hydrology and Earth System Sciences* 21, no. 3: 1559–1572.

Pickles, E. N. 2010. "Newton Wallis: The Evolution of a Landscape." *Yorkshire Archaeological Journal* 82, no. 1: 373–382.

Pregnolato, M., A. Ford, S. M. Wilkinson, and R. J. Dawson. 2017. "The Impact of Flooding on Road Transport: A Depth-Disruption Function." *Transportation Research Part D: Transport and Environment* 55: 67–81.

Rangari, V. A., N. Umamahesh, and C. Bhatt. 2019. "Assessment of Inundation Risk in Urban Floods Using HEC-RAS 2D." *Modeling Earth Systems and Environment* 5: 1839–1851.

Razavi, S., P. Gober, H. R. Maier, R. Brouwer, and H. Wheater. 2020. "Anthropocene Flooding: Challenges for Science and Society." *Hydrological Processes* 34, no. 8: 1996–2000.

Rudd, A. C., A. L. Kay, S. C. Wells, et al. 2020. "Investigating Potential Future Changes in Surface Water Flooding Hazard and Impact." *Hydrological Processes* 34, no. 1: 139–149.

Schilling, W. 1991. "Rainfall Data for Urban Hydrology: What Do We Need?" *Atmospheric Research* 27, no. 1–3: 5–21.

Singh, A., D. Dawson, M. A. Trigg, N. Wright, C. Seymour, and L. Ferriday. 2023. "Drainage Representation in Flood Models: Application and Analysis of Capacity Assessment Framework." *Journal of Hydrology* 622: 129718.

Singh, V. 1997. "Effect of Spatial and Temporal Variability in Rainfall and Watershed Characteristics on Stream Flow Hydrograph." *Hydrological Processes* 11, no. 12: 1649–1669.

Smith, A., P. D. Bates, O. Wing, C. Sampson, N. Quinn, and J. Neal. 2019. "New Estimates of Flood Exposure in Developing Countries Using High-Resolution Population Data." *Nature Communications* 10, no. 1: 1814.

Surendran, S., G. Gibbs, S. Wade, and H. Udale-Clarke. 2008. Supplementary Note on Flood Hazard Ratings and Thresholds for Development Planning and Control Purpose – Clarification of the Table 13.1 of FD2320/TR2 and Figure 3.2 of FD2321/TR1. Environment Agency and HR Wallingford.

Szeląg, B., R. Suligowski, G. Łagód, et al. 2022. "Flood Occurrence Analysis in Small Urban Catchments in the Context of Regional Variability." *PLoS One* 17, no. 11: e0276312.

Te Chow, V., D. R. Maidment, and L. W. Mays. 1988. *Applied Hydrology*. McGraw Hill.

Ten Veldhuis, M., Z. Zhou, L. Yang, S. Liu, and J. Smith. 2018. "The Role of Storm Dynamics and Scale in Controlling Urban Flood Response." *Hydrology and Earth System Sciences* 22, no. 1: 417–436.

Thorndahl, S., T. Einfalt, P. Willems, et al. 2017. "Weather Radar Rainfall Data in Urban Hydrology." *Hydrology and Earth System Sciences* 21, no. 3: 1359–1380.

US Army Corps of Engineers. 2020. HEC-RAS River Analysis System: HEC-RAS Mappers User's Manual [Computer Software Manual]. US Army Corps of Engineers.

Veneziano, D., and P. Villani. 1999. "Best Linear Unbiased Design Hyetograph." *Water Resources Research* 35, no. 9: 2725–2738.

Villalobos Herrera, R., S. Blenkinsop, S. B. Guerreiro, M. Dale, D. Faulkner, and H. J. Fowler. 2023. "Towards New Design Rainfall Profiles for the United Kingdom." *Journal of Flood Risk Management* 17: e12958.

Villalobos Herrera, R., S. Blenkinsop, S. B. Guerreiro, and H. J. Fowler. 2023. "The Creation and Climatology of a Large Independent Rainfall Event Database for Great Britain." *International Journal of Climatology* 43: 6020–6037.

Wang, Y., A. S. Chen, G. Fu, S. Djordjevi'c, C. Zhang, and D. A. Savić. 2023. "An Integrated Framework for High-Resolution Urban Flood Modelling Considering Multiple Information Sources and Urban Features." *Environmental Modelling & Software* 107: 85–95.

Watt, E., and J. Marsalek. 2013. "Critical Review of the Evolution of the Design Storm Event Concept." *Canadian Journal of Civil Engineering* 40, no. 2: 105–113.

Woods, R., and M. Sivapalan. 1999. "A Synthesis of Space-Time Variability in Storm Response: Rainfall, Runoff Generation, and Routing." *Water Resources Research* 35, no. 8: 2469–2485.

Yalcin, E. 2020. "Assessing the Impact of Topography and Land Cover Data Resolutions on Two-Dimensional HEC-RAS Hydrodynamic Model Simulations for Urban Flood Hazard Analysis." *Natural Hazards* 101, no. 3: 995–1017.

Yang, Y., L. Sun, R. Li, J. Yin, and D. Yu. 2020. "Linking a Storm Water Management Model to a Novel Two-Dimensional Model for Urban Pluvial Flood Modeling." *International Journal of Disaster Risk Science* 11: 508–518.

Yin, S.-Q., Y. Xie, M. A. Nearing, W.-L. Guo, and Z.-Y. Zhu. 2016. "Intra-Storm Temporal Patterns of Rainfall in China Using Huff Curves." *Transactions of the ASABE* 59, no. 6: 1619–1632.

Zhu, Z., D. B. Wright, and G. Yu. 2018. "The Impact of Rainfall Space-Time Structure in Flood Frequency Analysis." *Water Resources Research* 54, no. 11: 8983–8998.

Appendix A

Approximation of FEH Summer Design Profile

The FEH summer design storm profile is approximated using the method outlined in the FEH guidance (Kjeldsen 2007). Equation (A1) is applied for a 6h duration, 1-in-100 year return period event (with an accumulated rainfall depth of 59.29 mm for Lin Dyke; and 59.25 mm for Wyke Beck, as described in Section 2.3), where the proportional depth of rain, y, falling in the temporal proportion, x, of the total duration, centred on the peak is given as:

$$y = \frac{1 - a^z}{1 - a} \tag{A1}$$

where $z = x^b$, and a = 0.100 and b = 0.815 for the summer profile.

It is a known limitation of this formula that it gives unrealistically large values for the summer profile when a small timestep (i.e., a small value of x) is used. However, despite amendments being made to this formula since its initial publication, no supporting documentation of the implemented amendments are openly offered. Consequently, our approximation of the FEH rainfall curve has a slightly sharper and higher peak than that produced by ReFH2, and this presents a small limitation in our work.

Appendix B

Idealised Asymmetric Rainfall Profiles

In order to calculate the rainfall rate for an idealised asymmetric rainfall peak, the location of the peak is changed, but otherwise the shape of the rainfall profile is kept the same. To achieve this, we must effectively rescale the time axis both before and after the peak: for example, for a front-loaded event the rainfall curve before the peak is compressed, and the profile after the peak is stretched.

The fraction of rainfall before the peak f_* scales with the fraction of time before the peak $f_* = \left(t_{peak} - t_{start}\right) / \left(t_{end} - t_{start}\right)$. This is easy to see for a triangle-shaped rainfall profile, that is, one that linearly increases and decreases in intensity before and after the peak, but also applies to our profiles.

We define a rescaled time t_* , which is given as

$$t_* = \left(t - t_{peak}\right) / \left(t_{peak} - t_{start}\right)$$

when $t_{start} < t < t_{neak}$, in which case $-1 < t_* < 0$,

$$t_* = \left(t - t_{peak}\right) / \left(t_{end} - t_{peak}\right)$$

when $t_{peak} \le t < t_{end}$, in which case $0 \le t_* < 1$.

As an example, the profile of A/A_{total} for an event where $f_{\ast}=0.2$ is shown in Figure B1. Here, A_{total} is the total rainfall accumulation over the event.

The accumulation at a given scaled time t_* is given by the following equations, which are a generalisation of the FEH design storm profiles (the FEH design storm profiles correspond to $f_* = 0.5$).

$$\begin{split} A(t_*) = & A_{total} \left(f_* - f_* \frac{1 - a^{\left(-t_*\right)^b}}{1 - a} \right) \\ & \text{when } t_{start} < t < t_{peak}, \\ A(t_*) = & A_{total} \left(f_* + \left(1 - f_*\right) \frac{1 - a^{\left(t_*\right)^b}}{1 - a} \right) \\ & \text{when } t_{peak} \le t < t_{end}. \end{split}$$

The corresponding rainfall rate is calculated by numerically differentiating the accumulation curve on a minute-by-minute basis. Rainfall profiles for events with different values of f_{\ast} are shown in Figure 3a in the main text.

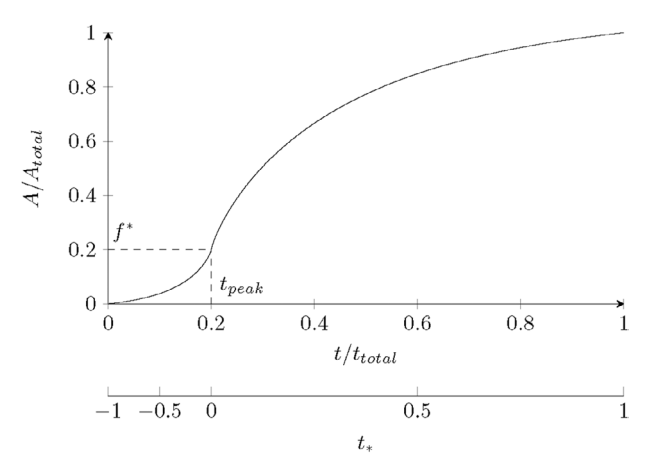


FIGURE B1 | Accumulated rainfall depth profile A/A_{total} for an asymmetric (front-loaded) rainfall event where $f_* = 0.2$.